Analysis and demonstration of atmospheric methane monitoring by mid-infrared open-path chirped laser dispersion spectroscopy

Nart S. Daghestani, Richard Brownsword, and Damien Weidmann*

Space Science and Technology Department, Rutherford Appleton Laboratory, Harwell Oxford Campus, Didcot OX11 0QX, UK

*damien.weidmann@stfc.ac.uk

Abstract: Atmospheric methane concentration levels were detected using a custom built laser dispersion spectrometer in a long open-path beam configuration. The instrument is driven by a chirped distributed feedback mid-infrared quantum cascade laser centered at ~1283.46 cm^{-1} and covers intense rotational-vibrational transitions from the fundamental ν_4 band of methane. A full forward model simulating molecular absorption and dispersion profiles, as well as instrumental noise, is demonstrated. The instrument's analytical model is validated and used for quantitative instrumental optimization. The temporal evolution of atmospheric methane mixing ratios is retrieved using a fitting algorithm based on the model. Full error propagation analysis on precision gives a normalized sensitivity of ~3 ppm.m.$Hz^{-0.5}$ for atmospheric methane.

OCIS codes: (300.6390) Spectroscopy, molecular; (300.6310) Spectroscopy, heterodyne; (140.5965) Semiconductor lasers, quantum cascade; (280.3420) Laser sensors.

References and links

1. G. Wysocki and D. Weidmann, "Molecular dispersion spectroscopy for chemical sensing using chirped mid-infrared quantum cascade laser," Opt. Express **18**(25), 26123–26140 (2010).
2. M. Nikodem, D. Weidmann, C. Smith, and G. Wysocki, "Signal-to-noise ratio in chirped laser dispersion spectroscopy," Opt. Express **20**(1), 644–653 (2012).
3. A. Hangauer, G. Spinner, M. Nikodem, and G. Wysocki, "Chirped laser dispersion spectroscopy using a directly modulated quantum cascade laser," Appl. Phys. Lett. **103**(19), 191107 (2013).
4. P. Martín-Mateos, B. Jerez, and P. Acedo, "Heterodyne architecture for tunable laser chirped dispersion spectroscopy using optical processing," Opt. Lett. **39**(9), 2611–2613 (2014).
5. M. Nikodem, G. Plant, Z. Wang, P. Prucnal, and G. Wysocki, "Chirped lasers dispersion spectroscopy implemented with single- and dual-sideband electro-optical modulators," Opt. Express **21**(12), 14649–14655 (2013).
6. D. J. Wuebbles and K. Hayhoe, "Atmospheric methane and global change," Earth Sci. Rev. **57**(3-4), 177–210 (2002).
7. D. R. Caulton, P. B. Shepson, R. L. Santoro, J. P. Sparks, R. W. Howarth, A. R. Ingraffea, M. O. Cambaliza, C. Sweeney, A. Karion, K. J. Davis, B. H. Stirm, S. A. Montzka, and B. R. Miller, "Toward a better understanding and quantification of methane emissions from shale gas development," Proc. Natl. Acad. Sci. U.S.A. **111**(17), 6237–6242 (2014).
8. D. M. D. Hendriks, A. J. Dolman, M. K. Van Der Molen, and J. Van Huissteden, "A compact and stable eddy covariance set-up for methane measurements using off-axis integrated cavity output spectroscopy," Atmos. Chem. Phys. **8**(2), 431–443 (2008).
9. S. M. Miller, S. C. Wofsy, A. M. Michalak, E. A. Kort, A. E. Andrews, S. C. Biraud, E. J. Dlugokencky, J. Eluszkiewicz, M. L. Fischer, G. Janssens-Maenhout, B. R. Miller, J. B. Miller, S. A. Montzka, T. Nehrkorn, and C. Sweeney, "Anthropogenic emissions of methane in the United States," Proc. Natl. Acad. Sci. U.S.A. **110**(50), 20018–20022 (2013).
10. J. Dobler, M. Braun, N. Blume, and T. S. Zaccheo, "A new laser based approach for measuring atmospheric greenhouse gases," Remote Sens. **5**(12), 6284–6304 (2013).
11. D. Miller, A. Michel, L. Stanton, K. Sun, L. Tao, and M. A. Zondlo, "Long open-path high precision quantum cascade laser methane sensing at Toolik Lake, Alaska," in *CLEO: 2013*, San Jose, California, OSA Technical digest (online) (2013), paper ATh1I.4.

#221540 - $15.00 USD Received 22 Aug 2014; revised 1 Oct 2014; accepted 18 Oct 2014; published 24 Oct 2014

12. G. Plant, M. Nikodem, D. M. Sonnenfroh, and G. Wysocki, "Chirped Laser Dispersion Spectroscopy for Remote Sensing of Methane at 1.65μm - Analysis of System Performance," in *CLEO: 2013*, San Jose, California, OSA Technical digest (online) (2013), paper JW2A.79.
13. B. Hirst, P. Jonathan, F. González del Cueto, D. Randell, and O. Kosut, "Locating and quantifying gas emission sources using remotely obtained concentration data," Atmos. Environ. **74**, 141–158 (2013).
14. B. Hirst, "A new approach to detecting, locating and quantifying surface gas fluxes above an onshore CO_2 storage project," in *11th Annual Conference on Carbon Capture Utilization and Sequestration*, Pittsburgh, Pennsylvania (2012).
15. L. S. Rothman, I. E. Gordon, A. Barbe, D. C. Benner, P. F. Bernath, M. Birk, V. Boudon, L. R. Brown, A. Campargue, J.-P. Champion, K. Chance, L. H. Coudert, V. Dana, V. M. Devi, S. Fally, J.-M. Flaud, R. R. Gamache, A. Goldman, D. Jacquemart, I. Kleiner, N. Lacome, W. J. Lafferty, J.-Y. Mandin, S. T. Massie, S. N. Mikhailenko, C. E. Miller, N. Moazzen-Ahmadi, O. V. Naumenko, A. V. Nikitin, J. Orphal, V. I. Perevalov, A. Perrin, A. Predoi-Cross, C. P. Rinsland, M. Rotger, M. Šimečková, M. A. H. Smith, K. Sung, S. A. Tashkun, J. Tennyson, R. A. Toth, A. C. Vandaele, and J. Vander Auwera, "The HITRAN 2008 molecular spectroscopic database," J. Quant. Spectrosc. Radiat. Transf. **110**(9–10), 533–572 (2009).
16. M. Nikodem, D. Weidmann, and G. Wysocki, "Chirped laser dispersion spectroscopy with harmonic detection of molecular spectra," Appl. Phys. B **109**(3), 477–483 (2012).
17. A. B. Carlson and P. Crilly, *Communication Systems*, 5th ed. (McGraw Hill, 2009).
18. D. Weidmann, W. J. Reburn, and K. M. Smith, "Retrieval of atmospheric ozone profiles from an infrared quantum cascade laser heterodyne radiometer: Results and analysis," Appl. Opt. **46**(29), 7162–7171 (2007).
19. J. Humlíček, "Optimized computation of the voigt and complex probability functions," J. Quant. Spectrosc. Radiat. Transf. **27**(4), 437–444 (1982).
20. L. S. Rothman, I. E. Gordon, Y. Babikov, A. Barbe, D. Chris Benner, P. F. Bernath, M. Birk, L. Bizzocchi, V. Boudon, L. R. Brown, A. Campargue, K. Chance, E. A. Cohen, L. H. Coudert, V. M. Devi, B. J. Drouin, A. Fayt, J.-M. Flaud, R. R. Gamache, J. J. Harrison, J.-M. Hartmann, C. Hill, J. T. Hodges, D. Jacquemart, A. Jolly, J. Lamouroux, R. J. Le Roy, G. Li, D. A. Long, O. M. Lyulin, C. J. Mackie, S. T. Massie, S. Mikhailenko, H. S. P. Müller, O. V. Naumenko, A. V. Nikitin, J. Orphal, V. Perevalov, A. Perrin, E. R. Polovtseva, C. Richard, M. A. H. Smith, E. Starikova, K. Sung, S. Tashkun, J. Tennyson, G. C. Toon, V. G. Tyuterev, and G. Wagner, "The HITRAN2012 molecular spectroscopic database," J. Quant. Spectrosc. Radiat. Transf. **130**, 4–50 (2013).
21. P. Werle, "Accuracy and precision of laser spectrometers for trace gas sensing in the presence of optical fringes and atmospheric turbulence," Appl. Phys. B **102**(2), 313–329 (2011).
22. Ebas database, http://ebas.nilu.no.
23. V. Simeonov, H. van den Bergh, and M. Parlange, "Long open-path TDL based system for monitoring methane background concentration for deployment at Jungfraujoch High Altitude Research Station - Switzerland," in *WMO Technical Conference on Meteorological and Environmental Instruments and Methods of Observation*, Helsinki, Finland, 30 Aug. - 1 Sept. (2010), paper P2(21).
24. K. Numata, H. Riris, S. Li, S. Wu, S. R. Kawa, M. Krainak, and J. Abshire, "Ground demonstration of trace gas lidar based on optical parametric amplifier," J. Appl. Remote Sens. **6**(1), 063561 (2012).

1. Introduction

Chirped Laser Dispersion Spectroscopy (CLaDS) has recently been established as a promising alternative method for high spectral resolution molecular gas sensing. With CLaDS, unlike sensing that relies on molecular absorption, dispersion profiles in the vicinity of a resonance are used to infer molecular density. In comparison to the widely used laser absorption spectroscopy approach, CLaDS brings unique benefits as far as molecular sensing is concerned. First, the use of dispersion allows for a far larger dynamic range than absorption when measuring mixing ratios. This is by virtue of the dispersion's linearity. Second, CLaDS signals stem from the phase alteration of electromagnetic fields, making the method more immune to laser intensity variations when compared with absorption spectrometers. Lastly, dispersion profiles are free of baseline. That specific feature lowers the dynamic range requirements placed upon the digital acquisition/processing hardware, and removes the need for baseline normalization.

The first demonstration of CLaDS was carried out using a tunable quantum cascade laser emitting around 5.23 microns. This seminal work was done by using a low pressure nitric oxide sample [1]. In the next step, the noise properties of this CLaDS spectrometer were empirically studied [2]. Further improvements and implementations of ClaDS were subsequently proposed [3–5]. In the present work, a CLaDS spectrometer developed to monitor methane samples in the mid-infrared in an open-path configuration is reported. The focus is placed on model development and validation, as well as error propagation, in order to establish a robust framework for the assessment of the spectrometer performance, primarily through the instrumental precision in this work. Assessment of experimental data against a

#221540 - $15.00 USD Received 22 Aug 2014; revised 1 Oct 2014; accepted 18 Oct 2014; published 24 Oct 2014

theoretical benchmark also facilitates the identification of excess noise impinging the instrument.

The rationale underpinning methane monitoring primarily relates to greenhouse gas monitoring in the Earth's atmosphere. Atmospheric methane concentrations have doubled since the start of the industrial revolution. It is estimated that two thirds of methane emission come from anthropogenic sources such as fossil fuel and biomass combustion, livestock ruminants, agricultural emission (rice cultivation), and waste decomposition. Natural sources include wetlands, permafrost, and termites [6]. Besides these established sources, the prospect of potential exploitation of shale gas has opened the need for monitoring over fracking sites, not to mention leak monitoring [7]. Whilst in situ monitoring provides valuable insights on methane concentrations and emissions [8, 9], most applications would benefit from sensors able to monitor over large distances, and/or large areas. In this respect, open-path sensing systems offer the advantage of measuring the integrated molecular mixing ratios over long lines of sight if needed. Using tomography [10] or meteorological data [11–14], the integrated mixing ratio degeneracy can be overcome and multidimensional information on mixing ratios of fluxes can be obtained in a cost effective manner. In a long beam path configuration, besides its usual molecular fingerprinting advantages, the mid-infrared illumination favors better propagation (less scattering), and relaxes eye-safety requirements.

The light source of the dispersion spectrometer hereby reported is a quantum cascade laser (QCL) whose emission covers rotational-vibrational transitions from the fundamental ν_4 band of methane centered at 7.7 μm. For the experiment, a bespoke laboratory-built electronics - acquisition-processing system has been developed in order to get full flexibility and control over the key parameters controlling the frequency information from which the molecular dispersion is obtained. The experimental apparatus is described in the first section. In the second section a full analytical model of CLaDS signal and noise is derived and validated. The purpose behind the model development consists of building robust analytical tools needed for concentration retrieval, prior analysis, and error and bias propagation. The model validation is carried out on a low pressure sample of methane mixture in laboratory conditions. In the last section, the demonstration of open-path atmospheric methane monitoring is presented.

2. Experimental implementation

The CLaDS spectrometer was set up in the laboratory with two purposes: 1) to carry out measurements on low pressure gas mixtures contained in a short path gas cell. This simple and well-controlled configuration was believed to be ideal for the validation of the instrument's theoretical model. 2) to conduct a set of initial atmospheric open-path experiments aiming to demonstrate performance and precision in a more realistic sensing configuration and compare with expectations. Figure 1 shows simplified optical layouts of for both configurations.

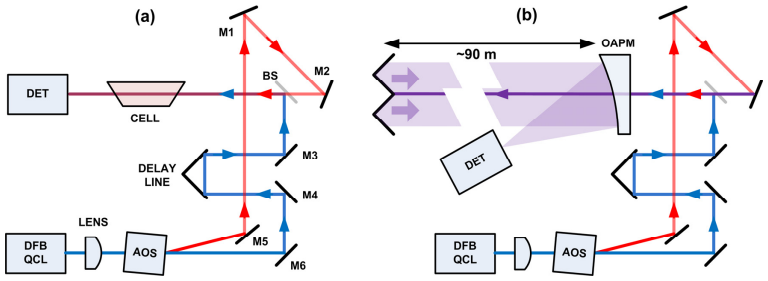

Fig. 1. Schematic of the CLaDS optical layout for (a) low pressure methane mixture experiments and (b) open-path atmospheric sensing.

The tunable laser source chosen for the spectrometer is a distributed feedback quantum cascade laser (Alpes Lasers SA), which exhibits a frequency tuning range covering 1278.4 to

#221540 - $15.00 USD Received 22 Aug 2014; revised 1 Oct 2014; accepted 18 Oct 2014; published 24 Oct 2014

1291.6 cm^{-1}. Within this range, the methane ro-vibrational transition centered at 1283.458791 cm^{-1} [15] is one of the most intense of the band (intensity of 6.256 10^{-20} cm^{-1}/molec.cm^2, which makes it the 6th most intense transition of the ν_4 band) whilst minimizing spectral interference from water that starts to significantly contribute near the edge of the 8-12 μm atmospheric window. The transition is accessible with the laser operating at ~25°C and producing ~20 mW of optical power.

The QCL is installed in a laboratory-built air-cooled laser module. It operates at an injection current of ~400 mA, with a compliance voltage of 8.6 V. The laser radiation is collimated by a 5 mm clear aperture aspheric lens with a numerical aperture of 0.56, producing a ~2 mm diameter beam with a close to Gaussian intensity distribution. The two fully coherent and frequency-offset fields needed to probe the sample dispersion are produced by a germanium acousto-optical shifter (AOS) driven at 95 MHz. The zeroth order beam exiting the acousto-optical crystal goes through an adjustable delay line, whilst the first order diffracted beam is directed to a beam steering assembly. Both beams are subsequently superimposed through a 50R/50T beamsplitter. The delay line is adjusted to ensure optical path equalization between the zeroth and first order beam. For experiments conducted on low pressure methane mixtures, the overlapped beams go through a 5 cm long glass cell (equipped with barium fluoride windows), and are directed onto a thermoelectrically cooled detector (PVI-2TE-10 from Vigo Systems) without focusing optics. For open-path experiments, the overlapped beams go through a 10 mm aperture made at the center of a gold-coated 30° off-axis parabolic mirror (OAPM) (101.6 mm diameter and 326.7 mm reflective focal length). Transmitted beams travel ~90 m towards a 127 mm aperture corner cube installed outdoors on a tripod. The part of the field returned to the instrument is focused onto the aforementioned detector. A visible green alignment laser collinear to the mid infrared radiation facilitates the alignment of the open-path configuration.

At the detector back-end, acquisition and radio-frequency processing is implemented through a custom made system. Signals from the detector are acquired by a 14 bit digitizer (Ultraview AD14-500 Series) at a fixed sampling rate of 500 MHz. An arbitrary waveform generator is synthesized by a universal software radio peripheral (Ettus Research USRP n210), which applies voltage waveforms to the modulation input of the QCL current driver. The carrier radio-frequency (RF) signal at 95 MHz that drives the AOS comes from a digital synthesizer (Ultraview SYNTH300). The 95 MHz carrier frequency also sets the central frequency of the bandpass filter in the FM demodulator described later. All sub-systems are synchronized and share a common 1 GHz timing signal. Once acquired by the digitizer buffer, the signals are software-processed. A LabView virtual instrument has been developed to control the system's inputs and outputs: the waveform signal that chirps the laser, the carrier signal frequency, radio-frequency signal processing, frequency demodulation, and filtering. The RF line is further described in the next section.

3. Signal and noise analytical model

3.1 FM signal and noise

A physical model describing the raw signals at the output of a CLaDS spectrometer has been reported in the seminal paper about the technique [1]. As far as noise is concerned, an empirical model of CLaDS noise properties was previously described in the case of nitric oxide detection [16] when using a commercial RF spectrum analyzer to carry out the frequency demodulation. Conversely, a purpose-built processing line offers a greater flexibility and control in selecting and optimizing the frequency demodulation parameters.

The noise model follows the development of Carlson and Crilly [17] on RF receivers. It is adapted to the specificities of the FM demodulation inherent to the CLaDS spectrometer. Otherwise, all assumptions underpinning the model of an RF receiver remain and are as follows: the noise power distribution at the output of the optical detector is white, the bandpass filters are assumed to be perfect top hat functions, all signals are assumed to be bandpass ones – meaning the variations of amplitude and phase are supposed to be slow

#221540 - $15.00 USD Received 22 Aug 2014; revised 1 Oct 2014; accepted 18 Oct 2014; published 24 Oct 2014

compared to the carrier frequency, signal and noise are independent of each other before the pre-detection bandpass filter, the carrier to noise ratio (CNR) is assumed to be much larger than one, and finally only narrow band FM is considered, for reasons to be detailed later.

The block diagram of the receiver back-end is shown in Fig. 2. An ideal receiver signal *x(t)*, originating from the heterodyne beating between the two overlapped beams, is delivered by an ideal photodiode. A white noise source of spectral density of $N_0/2$ is added to *x(t)* to emulate the inherent noise from the photodiode (and preamplifiers, which have not been represented in the schematic). The resulting signal passes through a bandpass filter (BPF) which selects the relevant intermediate frequencies. The BPF is assumed to be ideal with a full bandwidth of B_T (which can be set through the LabView virtual instrument) and a central frequency equal to the AOS driver frequency. The output filtered signal, denoted as *v(t)*, then undergoes FM demodulation. Demodulated signals are filtered by a low pass filters (LPF) assumed to be ideal with a full bandwidth of W_{FM} (also user-selectable).

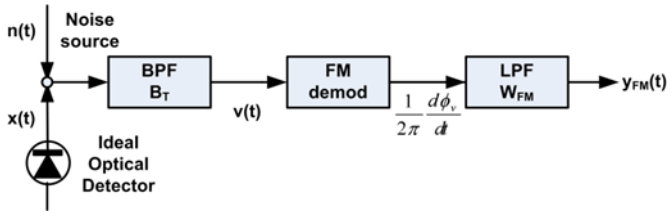

Fig. 2. Schematic of the radio-frequency processing line of the CLaDS instrument.

On the basis of this simplified block diagram the analytical equation describing the noise in the receiver can be derived. Firstly, the CNR prior to FM demodulation is given as the ratio of the received signal's power S_R to the noise power N_R within the reception bandwidth B_T. This can be expressed by Eq. (1):

$$CNR = \frac{S_R}{N_R} = \frac{S_R}{N_0 \cdot B_T} = \frac{A_c^2}{2N_0 \cdot B_T \cdot R_L} \tag{1}$$

The noise power N_R within the receiver bandwidth has been assumed to be solely attributed to the detector white noise. The received power has been expressed in terms of voltage amplitude A_c at the output of the optical detector (and preamplifier) coupled across a resistive load R_L.

The ideal narrow band FM noise within the demodulated signal, expressed in terms of standard deviation, is then given by Eq. (2). This equation takes into account the averaging of *k* samples, again under the assumption of a white noise limited system.

$$\sigma_{yFM} = \sqrt{\frac{{W_{FM}}^3}{3 \cdot CNR \cdot B_T \cdot k}} \tag{2}$$

The FM demodulated signal is recalled in Eq. (3) [1]. In this equation, *S* represents the laser chirp rate (assumed to be constant), Δ_L is the optical path difference between the 0th and 1st order beams combined to probe the molecular sample. In a well-adjusted CLaDS spectrometer, a zero baseline frequency signal is desirable; therefore a delay line is adjusted so that Δ_L remains zero. L_C is the path length over which the combined beams interact with the molecular sample. ω, Ω, *c*, and *n* are the optical angular frequency, the AOS frequency, the speed of light, and the sample refractive index, respectively.

$$f(\omega) = \frac{1}{2\pi}\left[-\frac{S \cdot \Delta L}{c} - \frac{S \cdot L_C}{c}\omega \cdot \left(\left.\frac{dn}{d\omega}\right|_{\omega-\Omega} - \left.\frac{dn}{d\omega}\right|_{\omega}\right)\right] \tag{3}$$

In order to establish the expression of the signal to noise ratio (SNR) from Eq. (2) and Eq. (3), various interdependences between already defined parameters need to be clarified. Firstly, the faster the laser scan rate over the molecular resonance, the larger the LPF must be in order

#221540 - $15.00 USD Received 22 Aug 2014; revised 1 Oct 2014; accepted 18 Oct 2014; published 24 Oct 2014

to capture the full extent of the relevant signal frequency components. In other words, the optimum LPF bandwidth W_{FM} is proportional to the laser chirp rate; let c_w be the proportionality term, where $W_{FM} = S \times c_w$. The term c_w depends on the specifics of the transition probed as well as on the pressure if collisional broadening is present. The optimum pre-detection bandwidth B_T of the BPF is also related to the LPF bandwidth through the Carson rule, given in Eq. (4). In the case of CLaDS, the modulation index β cannot be adjusted at will but is instead defined by the properties of the resonance being probed. In most cases, the modulation index remains well below unity. Therefore, the BPF bandwidth is usually set to twice the post detection LPF bandwidth.

$$B_T = 2(1+\beta)\cdot W_{FM} \approx 2\cdot W_{FM} \tag{4}$$

Lastly, within a fixed acquisition time, the number of samples that can be averaged k is also proportional to the laser chirp rate. The proportionality constant is defined to be c_k, where $k = S \times c_k$. The constant c_k is dependent on how efficiently the chirp is produced following the thermal heat release in the laser cavity induced by the current ramp. It depends on the tuning properties of a laser device, and in a lesser extent, on the electrical bandwidth of the current controller.

Accounting for the above described dependences, the SNR is given by Eq. (5), where the SNR is defined as the ratio of the maximum frequency deviation observed within the laser frequency scan to the noise. Δ_{MAX} is defined by Eq. (6) and depends on the rate of change of the refractive index of the sample, and the AOS frequency. The expression in Eq. (5) has been grouped into three terms: a set of constants, a set of parameters depending on the molecular resonance, and a set of parameters related to the optical detection hardware. It is interesting to note that ultimately the SNR is limited by the detector noise and by the RF power of the heterodyne beat note. The SNR can also be altered through the offset frequency. These expressions for noise and SNR have also dependence on the optical frequency ω, through the refractive index $n = n(\omega)$ and beat note RF power S_R. S_R is also related to the amount of absorption occurring within the sample, which varies with the optical frequency of the laser.

$$SNR = \frac{\sqrt{3}}{2\pi\cdot c}\cdot\frac{\omega\cdot\Delta_{MAX}(n,\Omega)\cdot\sqrt{c_k}}{\sqrt{c_W^3}}\cdot\sqrt{\frac{S_R}{N_0}} \tag{5}$$

$$\Delta_{MAX}(n,\Omega) = MAX\left[\left.\frac{dn}{d\omega}\right|_{\omega-\Omega} - \left.\frac{dn}{d\omega}\right|_{\omega}\right] \tag{6}$$

3.2 Full forward modelling

In a similar way to previously reported remote sensing instruments [18], a full forward modelling approach was implemented to get mixing ratios from the raw output spectra delivered by the CLaDS instrument. The full forward model also allows error propagation analysis and prior analysis of any sensing configuration to optimize design choices and instrument parameters on quantitative grounds.

The calculation of dispersion and absorption is performed by a line by line spectral model using the Humličeк algorithm in its complex format [19] to derive absorption and dispersion profiles of each molecular resonances occurring within the laser frequency sweep. HITRAN data are used as input parameter in the Humličeк algorithm [20]. Using Eq. (3), a synthetic temporal trace representing the expected CLaDS signal is calculated, as well as the expected ideal noise trace. The calculation of the noise involves the knowledge of the absorption spectrum since it affects the CNR through spectrally resolved reduction of transmitted power.

This first iteration of signal and noise calculation is then used to determine the optimum LPF bandwidth matching the specific input conditions of the model. Indeed, the LPF necessarily introduces a distortion of the actual molecular dispersion signal. One wishes to determine what the LPF bandwidth should be so that the distortion is negligible when compared to the noise level of the spectrum. The optimum LPF bandwidth must be redefined

#221540 - $15.00 USD Received 22 Aug 2014; revised 1 Oct 2014; accepted 18 Oct 2014; published 24 Oct 2014

whenever a parameter affecting the noise in the frequency demodulated signal is modified in order to maintain the above criterion. As a threshold, we set the LPF bandwidth as optimum when the amplitude distortion of the actual molecular dispersion signal remains three times smaller than the maximum one-sigma noise expected within the spectrum.

An error propagation algorithm is then added onto the forward model. It follows the generic formalism of the optimum estimation method [18]. The forward model can be simply described by Eq. (7), where y represents the measured CLaDS spectrum, x the parameters one wishes to measure (for example methane mixing ratios), b the ancillary parameters describing the instrument and the sensing configuration, and ε the measurement noise associated to y. The function f, describes the forward model containing all the physics known about the measurement.

$$y = f\left(x, b\right) + \varepsilon \tag{7}$$

Now, the process of inverting Eq. (7) to estimate x, in other words the retrieval process, can be represented by a function R and written as Eq. (8).

$$\hat{x} = R\left(y, \hat{b}, x_a, c\right) \tag{8}$$

$\hat{x}$ denotes the estimate of x rather than the true value, usually unknown. $\hat{b}$ also denotes estimates for ancillary parameters as some of them will be obtained from alternative sources with an associated confidence interval. x_a accounts for additional constraints that can be used in the form of a priori knowledge on the x values (for example local climatology of methane), and c takes into account parameters intrinsic to the retrieval process.

At a given state of input parameters describing the CLaDS monitoring configuration, the error can be described as how far the estimator $\hat{x}$ is from the true value x. As the scope is only placed on precision here, ignoring biases, the error on the measured values can be written directly as function of the measurement noise. Equation (9) gives the mathematical form of this.

$$\hat{x} - x = \frac{\partial R}{\partial y} \cdot \varepsilon \tag{9}$$

Hence, the local partial derivative of the retrieval process can be calculated to work out the sensitivity to instrument noise, and to turn the latter into the one-sigma uncertainty on the mixing ratio estimation. In future work, the full error derivation will be used to determine sensitivity of the mixing ratio measurements to any input parameter, thus accounting for biases and accuracy issues. Lastly, as this full forward model approach is based on global fitting and permits multi-parameter estimation, the error propagation module can help in determining potential cross-talk between retrieved parameters, which is another major source of inaccuracies to be explored in further studies.

4. Model validation

4.1 Inherent CLaDS noise

A set of CLaDS experiments was carried out in the laboratory in order to compare the model expectations with the measured data. At first, no molecular sample was introduced in the setup in order to characterize and validate the analytical noise model derived in the preceding section, inherent to the instrument alone. The dependence of the CLaDS frequency demodulated signal noise was investigated as a function of the parameters appearing successively in Eq. (2). The dependence of the noise on the post detection LPF bandwidth is shown in Fig. 3(a). For these measurements, the duration of the laser ramp was 10 µs, about 20 µW of optical power was reaching the detector, the laser chirp rate was 0.325 MHz/ns, and only a single trace was acquired (no averaging).

The noise spectral density N_0 at the output of the detector was measured to be 5.12 x 10^{-16} W/Hz. The assumption of a constant value over the BPF bandwidth is justified, given the

#221540 - $15.00 USD Received 22 Aug 2014; revised 1 Oct 2014; accepted 18 Oct 2014; published 24 Oct 2014

usually small BPF bandwidth with respect to the carrier frequency. In the plot of Fig. 3(a), the theoretical expectation is overlaid and indicates a fair match with the measurements. Small deviations from the model are to be expected given the number of assumptions made (particularly regarding the top-hat filter response functions) to derive the ideal case. Figure 3(b) shows the FM noise dependence on the number of averaged samples; a LPF with a bandwidth of 3.5 MHz was used, at a CNR of 46×10^3. For a large number of averaged samples, the noise reduction became less efficient due to drifts, making the white noise assumption no longer valid. This will be confirmed later using Allan variance analysis. When considering only the first six points, a linear fit on the log/log data returns a slope of -0.49 ± 0.02, and an intercept of 3.60 ± 0.03. The model predicts 0.5 and 3.52 respectively. Figure 3(c) shows the noise dependence on the last parameter involved in the noise definition, the CNR. The CNR was varied simply by controlling the amount of optical power reaching the detector. For these measurements the LPF bandwidth was set to 2 MHz and the BPF bandwidth to 5 MHz; all the other parameters were otherwise identical. A linear fit (on logarithmic scale) performed on the data returns a slope of -0.497 ± 0.004, where the model predicts -0.5, and an intercept of 5.60 ± 0.02 where 5.86 would be expected. The discrepancies arise primarily from the assumptions made on the filter shape and bandwidth estimates, as for in Fig. 3(a). This series of measurements of noise inherent in CLaDS appears to be well described by the analytical model. In a next step, a molecular sample is introduced to carry on the modelling by introducing a dispersion signal and the associated signal to noise ratio.

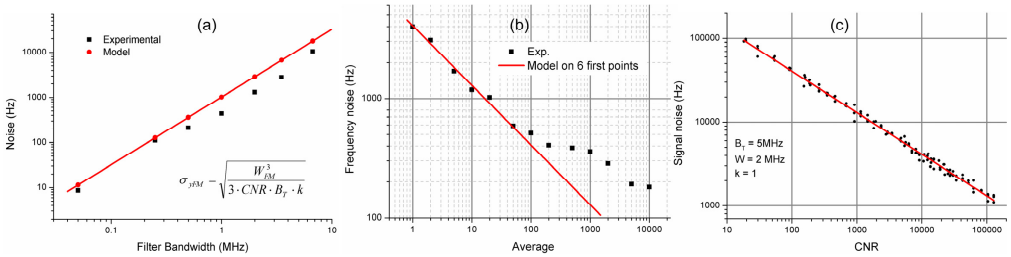

Fig. 3. (a). Dependence of the noise in the FM demodulated CLaDS signal as function of the post detection LPF bandwidth (single cycle data). (b) Dependence of the noise with the number of averaged samples. The solid line indicates the model. (c) Dependence of the noise of the FM demodulated CLADS signal as function of the CNR.

4.2 Low pressure molecular measurements

Before starting the open-path measurements of atmospheric methane, low pressure samples of methane diluted in nitrogen were investigated under controlled laboratory conditions, and measurements were compared with the model. A 5cm-long gas cell was introduced in the path of the combined beams. The cell was filled with 24 Torr of a mixture containing $(1.3 \pm 0.2)\%$ of methane diluted in dry nitrogen. The laser was chirped at 0.354 MHz/ns across the transition of methane centred at 1283.458791 cm^{-1}. The chirp was produced by application of a 10 µs current ramp to the QCL, the LPF was set at 3.9 MHz, the BPF at 7.8 MHz. The CNR was 83×10^3. 500 traces were averaged. The experimental methane spectrum obtained in these conditions is given in Fig. 4(a), onto which the fitted model is overlaid. Individual traces can barely be distinguished, therefore the lower panel shows the residual expressed as per cent of the maximum of the CLaDS signal. The residual is mostly random noise, except around the dispersion profile where mismatch up to ~3% are observed. The fitting algorithm returned a methane concentration of (1.3053 ± 0.0004) %.

To carry out Allan variance analysis [21] on the measured mixing ratios, low pressure methane spectra were acquired repeatedly at a rate of one spectrum every 1s. The chirp rate was 50 kHz/ns, single cycle, CNR was 9×10^5, the total acquisition time for a single scan was 150 µs, made of a 100 µs current ramp, and a 50 µs waiting time. The LPF was set at 0.5

#221540 - $15.00 USD Received 22 Aug 2014; revised 1 Oct 2014; accepted 18 Oct 2014; published 24 Oct 2014

MHz, and the BPF at 1 MHz. The acquisition – processing chain, taking into account the demodulation calculation time, can allow a maximum number of 70 averaged traces whilst still maintaining the temporal resolution of one spectrum per second. Experiments were run both in single trace acquisition and 10 traces averaged. Each spectrum was fitted to retrieve the methane mixing ratio. From this temporal record, the Allan deviation was derived and is shown in Fig. 4(b), in which normalization to one second has been done. Drifts, most likely thermal, take over the random noise after about ~100 s. The maximum achievable limit of detection in these particular conditions is 60 ppb.m.

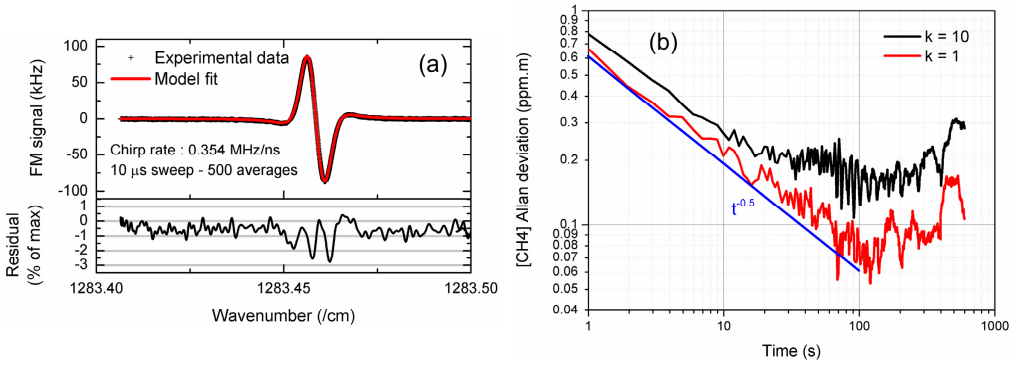

Fig. 4. (a). Low pressure CLaDS spectrum for the transition of methane centered at 1283.458791cm^{-1}. The sample was 1.3% methane in a 5 cm long cell, the CNR was 83 × 10^3, the total acquisition time was 10 ms. The model was fitted to the experiment. Residual expressed in percent of the maximum CLaDS signal is given in the lower panel. (b) Allan deviation for a 1200 s record of methane concentrations at a rate of one measurement per second, for a single trace acquisition (150 µs scan time) and 10 averaged traces, both normalized to one second.

In a next series of measurements, the dependence of the concentration error on the CNR was assessed through comparison with the calculated ones under the ideal conditions of the forward model. The CNR was experimentally varied using a polarizer to alter the laser power falling onto the detector. The results are shown in Fig. 5(a). Scatter plots relate to the experimental data whilst solid lines are obtained from the modelling. The match between both is fairly good and therefore indicates that the CLaDS system mostly operates close to the detector-noise-limited case. At high CNR (>10,000), and significant averaging (1000 traces, though still within the stability limit indicated by the Allan variance analysis), the methane mixing ratio precision seems to hit a floor, not accounted for in the model. As the FM demodulation noise is reduced, excess noise sources that were not significant otherwise start to appear and limits further reduction of the limit of detection.

Several excess noise sources have been identified. First, the dominant one relates to the digital frequency demodulation process. Because of the limited time window encompassing the signal, residual oscillations are produced in the demodulation trace. Usually, removing the first 20% of the demodulated signal addresses the issue, though at very low LPF (≤50 kHz, relevant to atmospherically-broadened transitions), these oscillations can contribute as a very slight baseline in the CLaDS spectra. Second, at high CNR (>30,000), excess RF noise has been observed in the detected signal, in the range of 28 nW of noise power per MHz of bandwidth and per W of carrier power. Lastly, spurious optical standing waves produce additional noise, as already reported [2], though these have been largely minimized by using wedged transmission optics and introducing a deliberate misalignment to the beam incident onto the acousto-optical shifter. The latter has been identified to be the major contributor to standing waves primarily because the 8-12 µm broadband antireflection coating reflects a few percent at the laser wavelength of 7.7 µm. Its standing wave component was reduced more than 20-fold by slightly tilting the crystal in the direction normal to the incident plane.

#221540 - $15.00 USD Received 22 Aug 2014; revised 1 Oct 2014; accepted 18 Oct 2014; published 24 Oct 2014

Using the same methane sample, with all the other parameters being fixed, the SNR as function of CNR was recorded to exhibit the threshold effect expected in FM detection [17]. Figure 5(b) shows the measurement. The LPF bandwidth was set to 3.5 MHz, and the BPF to 7 MHz. The chirp rate was 0.325 MHz/ns. Two sets of data are shown, one without averaging, the other with 200 spectra averaged. The dependence of SNR as function of CNR is as expected from the model except for a clear threshold effect. This effect is expected from a FM demodulation process, in which the phase of the signal to demodulate can be overwhelmed by noise to a point where the demodulation can no longer retrieve information [17].

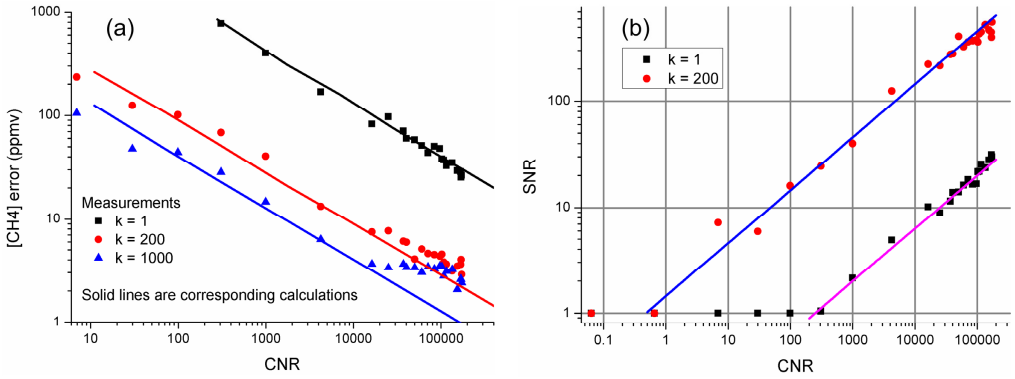

Fig. 5. (a). One-sigma precision on CH_4 mixing ratios measurements as function of the CNR. These were obtained from a ~1.3% methane mixture in N_2, 5 cm cell length, 24 Torr total pressure, 0.325 MHz/ns, and a post detection LPF of 3.5 MHz. Several averaging conditions were recorded. The corresponding solid lines shows the expected detector noise-limited precision calculated from the CLaDS signal and noise models, using error propagation analysis. (b) Evolution of the SNR as function of the CNR exhibiting a threshold effect (single cycle data and 200 averages).

This concludes the full model validation of the CLaDS system and demonstrates that under low pressure sample conditions, in the controlled environment of the laboratory, the spectrometer operates as an ideal detector noise-limited sensor, notwithstanding the excess noise limitations highlighted in Fig. 5(a).

5. Long-path atmospheric methane measurements

Following the establishment and validation of the physical signal and noise model describing the CLaDS system, a first open-path demonstration in the atmosphere was carried out. The experimental system has already been described in the second section. The open-path length was measured to be 181.75 ± 0.06 m, using a telemeter. The power transmitted was ~5.8 mW, and the power received was in the range of 230 μW. The collimated laser beam has a full angle divergence calculated to be 1.66 mrad from the assumed laser facet properties and the lens specifications. This means the 99% encircled energy diameter after 180 m propagation is in the order of 450 mm, largely overfilling the collection mirror. As a result, the system was found to be insensitive to misalignments, whilst still providing plenty of optical power, even sufficient to even saturate the detector. Therefore longer path lengths can be accommodated and the system was limited to ~90 m distance by the topography of the campus, which restricted the line of sight accessible from our laboratory windows.

A time series of methane mixing ratios has been measured over 2 hours. The experimental conditions were as follows: chirp rate of 37 kHz/ns, 100 averaged spectra, 1 ms current ramp, LPF bandwidth of 32 kHz, CNR of ~110×10^3. During the measurements, the outdoor temperature was 283.5 K, the ambient pressure was 763 Torr, and the water vapour concentration was 9500 ppmv.

A single CLaDS spectrum extracted from the series is shown in Fig. 6(a). The laser frequency was swept over ~1 cm^{-1}, encompassing three methane transitions. Overlaid on the experimental spectrum is the fitted model that returned a 15 ppb precision on the

#221540 - $15.00 USD Received 22 Aug 2014; revised 1 Oct 2014; accepted 18 Oct 2014; published 24 Oct 2014

determination of the methane mixing ratio. The residual is shown in the corresponding lower panel. As a comparison, the fully calculated traces, using the previously described model, are shown in Fig. 6(b), in which the lower panel shows the simulated noise trace. The measured noise is about two times larger than expected under fully ideal conditions of a detector noise-limited system. Lastly, Fig. 6(c) shows the calculated individual signals from the three contributing molecules, which are included in the model.

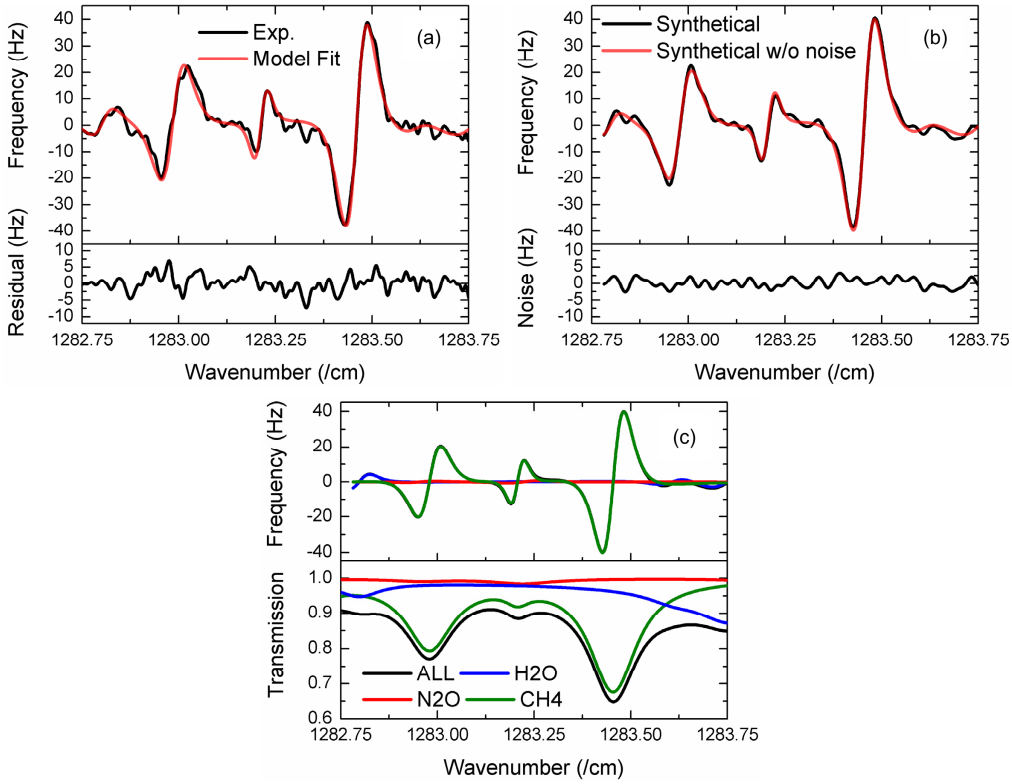

Fig. 6. (a). Experimental spectrum extracted from the open-path time series measurements. Both the experimental data and the model fit are show. (b) Corresponding full modelling of the spectrum, including simulated noise. (c) Calculated individual contributions from the three atmospheric molecules integrated into the model. CLaDS dispersion signal (top panel) and transmission (bottom) are shown.

The full time series of methane mixing ratio is shown in Fig. 7. For this open-path demonstration, no other alternate instrument was available for cross-validation of the data series. Therefore the accuracy of the measurements cannot be assessed. However, based on methane data recorded by existing ground stations, mixing ratios look realistic [22]. Validation of the measured data against different sensors, along with a full accuracy analysis will be the scope of future work.

From low pressure methane mixtures to atmospheric open-path experiments, collisional line broadening results in much wider resonances. It has been established that the CLaDS demodulated frequency signal is maximized when the frequency difference between the overlapped probe beams matches the FWHM of the transition [1]. Using the model described above, this effect is taken into account through Eq. (6). Under the conditions of the open-path experiment, Fig. 8(a) shows the effect of varying the frequency difference Ω on the SNR and the error on methane mixing ratios. Currently, the experimental CLaDS system uses an AOS to produce a 95 MHz frequency difference.

The plot in Fig. 8(a) indicates that increasing Ω to ~80% of the resonance full width (about 3400 MHz) would bring the precision 13 times higher. Alternative approaches to

#221540 - $15.00 USD Received 22 Aug 2014; revised 1 Oct 2014; accepted 18 Oct 2014; published 24 Oct 2014

acousto-optical shifting are required to achieve the optimum frequency difference; for example direct laser modulation for side bands creation has been attempted [5]. Frequency difference that matches collisionally broadened lines at atmospheric pressure remains very demanding for the acquisition system in terms of speed. A trade-off between sensitivity and complexity ought to be made in each sensing case, and the model described in this paper has been partly developed for such a purpose.

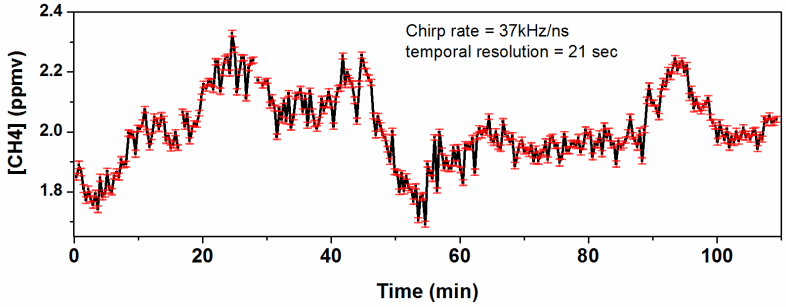

Fig. 7. Temporal evolution of methane mixing ratio as measured by the open-path CLaDS spectrometer.

Lastly, Fig. 8(b) summarizes the precision obtained with measurements done both in a low pressure sample and in the open-path configuration. In addition, the dependence of the precision (and hence the SNR) with the laser chirp rate is shown. According to Eq. (5) there should be no dependence of sensitivity to the chirp rate. This is seen almost to be the case. A slight variability is observed (~35%); however, accounting for the fact that the chirp rate is varied by four orders of magnitude, this variability is attributed to second order instrumental effects deviating from ideal conditions.

In addition to the experimental data, extrapolated data have been shown in Fig. 8(b). Currently the filtering and demodulation is done via a LabView program and is far from being time efficient. The extrapolation shows what could be expected from a quasi-real time digital signal processor that would increase the number of spectra averaged per second to the maximum amount allowed by a given chirp rate.

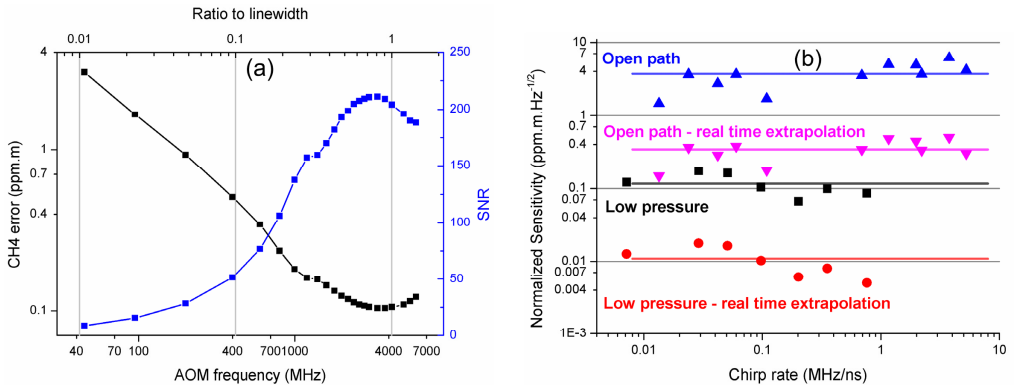

Fig. 8. (a). Calculations of SNR and methane mixing ratio error as function of the difference frequency Ω. The top x axis shows the ratio of Ω to the full width at half maximum of the most intense CH_4 transition in the scan range. (b) Single scan normalized experimental sensitivity as function of the laser chirp rate for open-path and low pressure methane mixing ratio measurements. Extrapolation of the experimental data to real time data processing has been included.

Even without a real-time processor, the open-path CLaDS instrument operates at a level of high sensitivity as far as long open-path methane monitoring is concerned. For example, an open-path instrument using wavelength modulation absorption spectroscopy and QCL at 8

#221540 - $15.00 USD Received 22 Aug 2014; revised 1 Oct 2014; accepted 18 Oct 2014; published 24 Oct 2014

μm has been deployed over 229 m and exhibited a ~4.6 ppm.m.$Hz^{-0.5}$ precision [11]. This is slightly lower than the best performance obtained with the CLaDS instrument (See Fig. 8(b)). Elsewhere, using VCSEL tunable diode laser and direct absorption spectroscopy in the harmonic band of methane at 1654 nm, an estimated precision of ~3 ppm.m.$Hz^{-0.5}$ is claimed [23]. This estimate is similar to the precision of the mid infrared CLaDS system, the latter being more resilient to atmospheric scattering. Lastly, a lidar system based on optical parametric oscillator and measuring methane in the 3.3 μm fundamental bands was recently reported [24]. The precision is not reported as such but can be estimated to be >100 ppm.m.$Hz^{-0.5}$ from temporal methane measurement series. The instrument has been tested on cooperative reflective targets rather than a proper mirror-based retro-reflector, which might contribute to the significant difference in precision compared to the CLaDS system.

6. Conclusion and future work

Driven by the increasing requirements for greenhouse gas monitoring, an open-path mid-infrared spectroscopic sensor has been presented, relying on Chirped Laser Dispersion Spectrometry with a quantum cascade laser as the spectroscopic source. Alongside the experimental implementation, a full physical model of the instrument, including signal and noise has been developed and is shown to be well validated via laboratory experiments. The validation was made using low pressure methane sample for which precision level down to ~100 ppb.m.$Hz^{-0.5}$ have been obtained. Using the model, to which an additional error propagation module has been added, the CLaDS spectrometer was found to be detector noise limited providing the product of CNR by number of averaged spectra remains below 10^7. Subsequently, open-path monitoring of methane in the atmosphere over an integrated range of 90 m has been demonstrated with a normalized precision of ~3 ppm.m.$Hz^{-0.5}$. Full forward modelling demonstrated that performance was degraded by a factor two with respect to the ideal case of detector-noise-limited operation.

The validated physical model can now be used operationally to benchmark actual measurement performance and/or carry out prior analysis in any CLaDS sensing scenario. It allows the systematic determination of optimized instrumental parameters based on quantitative precision estimates. In future work, it will also be used to investigate accuracy and biases of the instrument.

Acknowledgments

This work has been supported by a proof of concept award from STFC Innovations Ltd. The authors wish to thank Gary Williams, from the Space Science and Technology Department, for his technical help. Andrew Larkins from Lime Tree Innovation Ltd is also acknowledged for his contribution in developing the custom made RF processing line.